Journal of Power Sources 270 (2014) 312–317

Contents lists available at ScienceDirect

Journal of Power Sources

journal homepage: www.elsevier.com/locate/jpowsour

Utilization of corn cob biochar in a direct carbon fuel cell

Jinshuai Yu, Yicheng Zhao, Yongdan Li*

Collaborative Innovation Center of Chemical Science and Engineering (Tianjin), Tianjin Key Laboratory of Applied Catalysis Science and Technology, State Key Laboratory of Chemical Engineering (Tianjin University), School of Chemical Engineering and Technology, Tianjin University, Tianjin 300072, China

HIGHLIGHTS

- Corn cob biochar is prepared with a pyrolysis process.
- Electrochemical performance of the biochar is examined in DCFC.
- Boudouard reaction takes part in the anode mechanism.
- Biochar is suitable for DCFC.

GRAPHICAL ABSTRACT

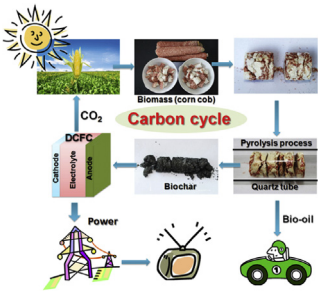

ARTICLE INFO

Article history:
Received 27 May 2014
Accepted 19 July 2014
Available online 24 July 2014

Keywords:
Direct carbon fuel cell
Biomass
Carbon cycle
Composite electrolyte

ABSTRACT

Biochar obtained from the pyrolysis of corn cob is used as the fuel of a direct carbon fuel cell (DCFC) employing a composite electrolyte composed of a samarium doped ceria (SDC) and a eutectic carbonate phase. An anode layer made of NiO and SDC is utilized to suppress the cathode corrosion by the molten carbonate and improves the whole cell stability. The anode off-gas of the fuel cell is analyzed with a gas chromatograph. The effect of working temperature on the cell resistance and power output is examined. The maximum power output achieves 185 mW cm^{-2} at a current density of 340 mA cm^{-2} and 750 °C. An anode reaction scheme including the Boudouard reaction is proposed.

1. Introduction

A huge amount of biomass is produced every year by nature through photosynthesis with solar energy from CO_2 and H_2O. Biomass and its fossil deposits actually provide the basic necessities in people's daily life including food, clothe, house and medication [1]. Biomass utilization as an energy source generates significantly less CO_2 than that of fossil fuels since its formation is a part of the carbon cycle in nature [2–6]. Biomass has been converted in a number of ways to produce biofuels [7,8]. Among them, pyrolysis has a very long history and has been improved and widely used to produce coke and charcoal [9]. In recent years, pyrolysis of biomass, a thermal decomposition process in nature, is employed to obtain bio-oil and biochar [7–9]. The bio-oil is further modified to transportation fuel and the biochar can be burned to produce electricity and heat [6]. However, the efficiency of energy utilization of biochar is low if direct combustion and thermal transformation processes are applied.

Direct carbon fuel cell (DCFC) converts the chemical energy stored in solid carbon into electricity directly without the reforming and thermal cycle processes [10–12]. The overall cell reaction of a DCFC can be considered as the electrochemical oxidation of carbon in the anode with releasing CO_2 ($C + O_2 = CO_2$). Due to a near zero entropy change ($\Delta S = 1.6$ J K^{-1} mol^{-1} at 600 °C), DCFC has a theoretical thermal efficiency approaching 100% and a practical

* Corresponding author. Tel.: +86 22 27405613; fax: +86 22 27405243.
E-mail address: ydli@tju.edu.cn (Y. Li).

http://dx.doi.org/10.1016/j.jpowsour.2014.07.125
0378-7753/

efficiency of around 80% [11]. Solid carbon fuels have a wide diversity and can be derived from either fossil or bio sources. Many kinds of carbon fuels have been tested in DCFC with various configurations [13]. Cherepy et al. [10] studied the electrochemical oxidation performance of carbon fuels in a molten carbonate fuel cell (MCFC) and reported that three important factors of carbon, including crystallographic disorder, electrical conductivity and adequate reactive surface sites, influence the cell power output. Direct conversion of carbon in a solid oxide fuel cell (SOFC) has also been explored and the effect of contact between anode and carbonaceous fuels was discussed [14].

Both solid oxide and molten carbonate materials have been used as the electrolyte of DCFC. Zhu et al. [15] demonstrated the high ionic conductivity of the composite electrolytes, composed of a oxide ion conducting semiconductor and a molten salt phase, in intermediate temperature range, *i.e.* 400–700 °C. Xia et al. [16,17] utilized the composite electrolyte to compose a very efficient fuel cell with hydrogen as the fuel. Jia et al. [18] utilized further the conductivity and reactivity of the molten carbonate with nanocarbon and constructed a DCFC with an anode composed of carbon in molten carbonate suspension, which was elaborated with a kinetic model by Li et al. [19]. More recently, Jiang et al. [20] extended the concept and proposed a hybrid fuel cell utilizing a solid oxide phase as the electrolyte and a carbon in molten carbonate anode. With their configuration, the thickness of the electrolyte can be effectively reduced. In our recent works, the DCFCs with different carbon fuels have been investigated and effort was made to improve the output with modifying the configuration [21–26].

To achieve the goal of clean and efficient utilization of biomass to generate electricity, in this work, corn cob biochar is used as the fuel of the DCFC based on a composite electrolyte. The cell exhibits promising performance in a temperature range of 650–750 °C.

2. Experimental

2.1. Preparation of the fuel and the fuel cell materials

Corn cobs were broken into small pieces and pressed into pellets. The pellets were subsequently heated in a quarz tube at 700 °C in N_2 with a flow rate of 50 ml min^{-1} (STP) for 2 h. Bio-oil and biochar were obtained during the pyrolysis process. The yield of biochar is 25 wt. % on dry base.

$Ce_{0.8}Sm_{0.2}O_{1.9}$ (SDC) powder was prepared with an oxalate co-precipitation method as described in previous work [16]. Li_2CO_3 and Na_2CO_3 powders with a mol ratio of 2:1 were ball milled for 4 h and then heated at 700 °C in air for 1 h to obtain a binary carbonate eutectic. SDC powder and the eutectic salt were mixed with a weight ratio of 7:3 and calcined at 700 °C in air for 1 h to form a composite material. A mixture of LiOH and NiO with a mol ratio of 1:1 was sintered at 700 °C in air for 2 h to prepare the lithiated NiO. A mixture of lithiated NiO and the composite electrolyte with a weight ratio of 7:3 was heated at 700 °C in air for 2 h to obtain the cathode material. A mixture of SDC and NiO with a weight ratio of 4:6 was sintered at 700 °C in air for 2 h to prepare the anode material.

The pellet containing an electrolyte layer and a cathode layer was fabricated with a co-pressing method followed by sintering as described in previous work [18,22]. The anode material was made into a slurry with a binder (10% ethyl cellulose + 90% terpineol), and then screen-printed on the electrolyte layer followed by sintering at 700 °C in air for 1 h to form the three-layer cell pellet. Ag paste was coated on both sides of the pellet as the current collector. The fuel was a mixture of biochar and the eutectic salt with a weight ratio of 1:9, which was put in the anode cavity on top of the pellet before the performance test.

2.2. Characterization

The surface morphologies of biochar and the single cell were characterized with a Hitachi S-4800 scanning electron microscope (SEM). The X-ray diffraction (XRD) pattern of the biochar was recorded with Bruker AXS, D8-S4 equipment using Cu Kα radiation. Thermogravimetric analysis (TGA) of the biochar was conducted in air with a flow rate of 50 ml min^{-1} (STP) and a heating rate of 10 °C min^{-1} from room temperature to 1000 °C in a NETZSCH STA, 449F3 instrument.

2.3. Fuel cell test

The anode off-gas was analyzed using an online gas chromatograph (Clarus 500, Perkin Elemer) with a thermal conductivity detector. The electrochemical impedance spectroscopy (EIS) of the fuel cell was measured at open circuit voltage (OCV) in a temperature range of 600–750 °C using an electrochemical workstation (Versastat 3, Princeton Applied Research) in a frequency range of 100 KHz to 0.1 Hz. The performance of the single cell was tested in a temperature range of 600–750 °C under atmospheric pressure with a similar configuration as in the published work [18]. Nitrogen was used as the anode protective gas with a flow rate of 100 ml min^{-1} (STP) and the cathode gas was a mixture of CO_2 (120 ml min^{-1}, STP) and O_2 (60 ml min^{-1}, STP). The heating rate of the fuel cell was 5 °C min^{-1}. The *I–V* characteristics of the single cell were measured with the electrochemical workstation with a scan rate of 10 mV s^{-1}.

3. Results and discussion

3.1. Properties of the biochar

Fig. 1(a) is a photo of the corn cob pieces used in this work. After pyrolysis, the biochar was obtained as shown in Fig. 1(b). The surface morphology of the biochar illustrated in Fig. 1(c) is very similar to the activated carbon from coconut used in our previous work [18]. Pores can be found on its surface, which enlarge the surface area and provide more electrochemical reaction sites.

Two weak broaden peaks are observed in the XRD pattern of biochar at around $2\theta = 24^\circ$ and $2\theta = 44^\circ$ (Fig. 2). The first peak is attribute to the (0 0 2) reflection and the other is the (1 0 0) reflection of graphite crystal. The average stacking height (L_c) and the average diameter (L_a) of biochar can be calculated according to the Scherrer equation [$L_c = 0.89\lambda/(B_{(002)}\cos\theta)$, $L_a = 1.84\lambda/(B_{(100)}\cos\theta)$], where λ is the wavelength of the X-ray beam, B is the peak width at half-maximum intensity, and θ is the Bragg angle [27]. Unlike carbons with high crystallinity such as graphite and carbon fiber, the self-made biochar has a more disordered structure (L_c is 1.1 nm and L_a is 3.8 nm). With high concentration of edge atoms, biochar is easy to be oxidized in the chemical reaction. Meanwhile, less graphitized carbon is also favorable in the electrochemical reaction for getting high performance [10,19].

A slight weight loss of the biochar below 150 °C is observed in the TGA curve (Fig. 3), which is due to the vaporization of water and other volatile substance absorbed in the sample. The oxidation of the biochar started at about 290 °C. The oxidizing rate increases with the increase of the operating temperature, and reached the maximum at 516 °C, as shown in the differential thermogravimetry (DTG) curve. Above 590 °C, the carbon in the sample was completely oxidized to CO_2, and the residual, about 3.98 wt. % of the biochar, was the ash component. Compared to the carbon materials

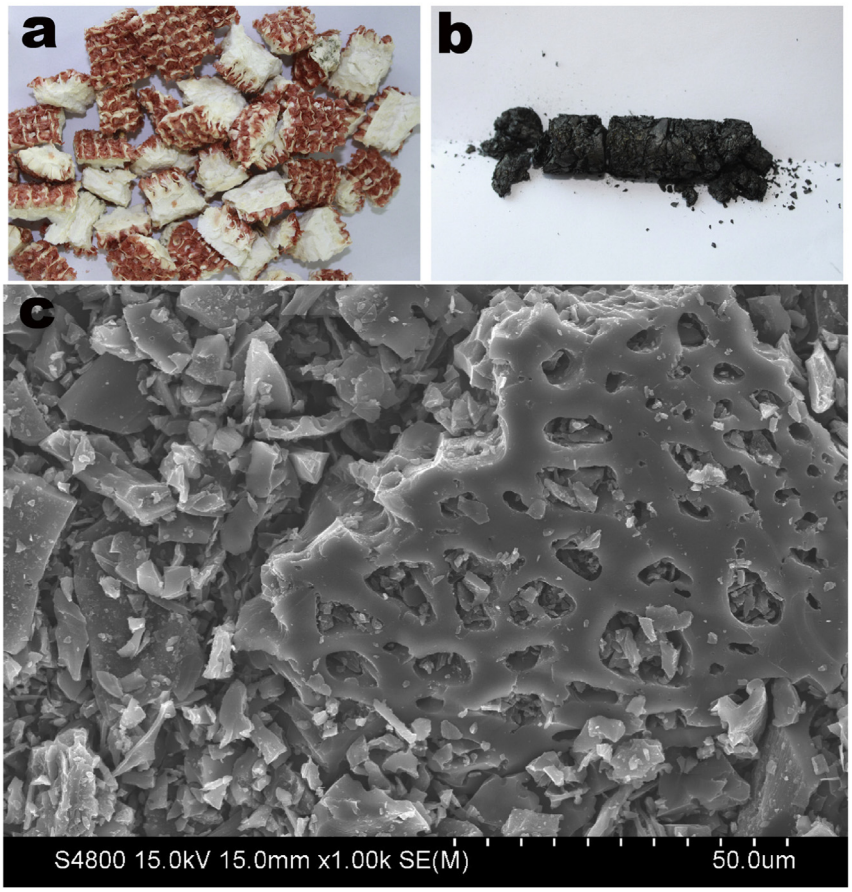

Fig. 1. (a) Photo of the corn cob. (b) Photo of the biochar. (c) Surface morphology of the biochar.

with high crystallinity such as graphite and carbon fiber [22], the biochar here is easier to be oxidized, implying a high electrochemical reacting rate in the anode of the DCFC [23,28].

3.2. Fuel cell analysis

3.2.1. SEM analysis

The surface morphologies of the fuel cell materials are illustrated in Fig. 4. The thickness of the printed anode layer is less than 10 μm as shown in Fig. 4(a). Fig. 4(b) reveals that the anode layer has a good fitting with the molten carbonate phase, which means that the printed anode layer may help to hold the molten carbonate and reduce the carbonate leakage from the anode fuel mixture to the cathode side. Compared to the two-layer cell pellet in the previous work [18], the cathodic corrosion by the carbonate is alleviated and the stability of the fuel cell has been improved. SDC particles are dispersed in the molten carbonate continuous phase in the electrolyte layer (Fig. 4(c)). The composite electrolyte provides the channels for the transfer of both O^{2-} and CO_3^{2-} ions. Fig. 4(d) shows that the lithiated NiO particles and SDC/MC particles are well mixed in the cathode, and the porous structure facilitates the diffusion of the cathode gas [29].

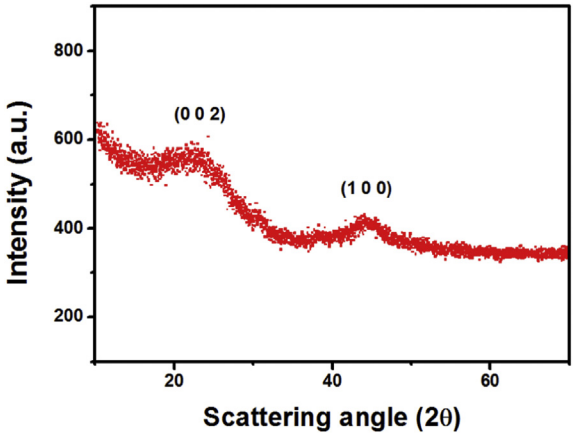

Fig. 2. XRD pattern of the biochar.

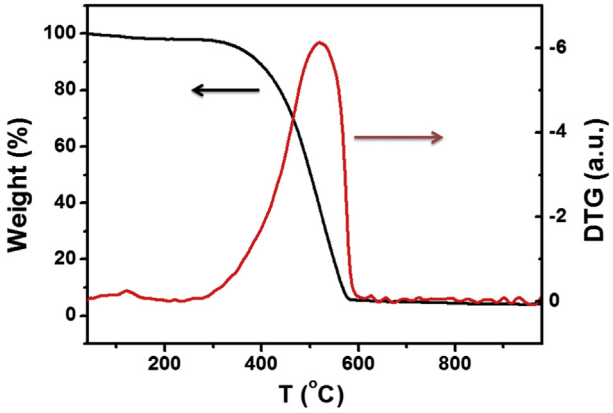

Fig. 3. TG and DTG curves of the biochar in air atmosphere.

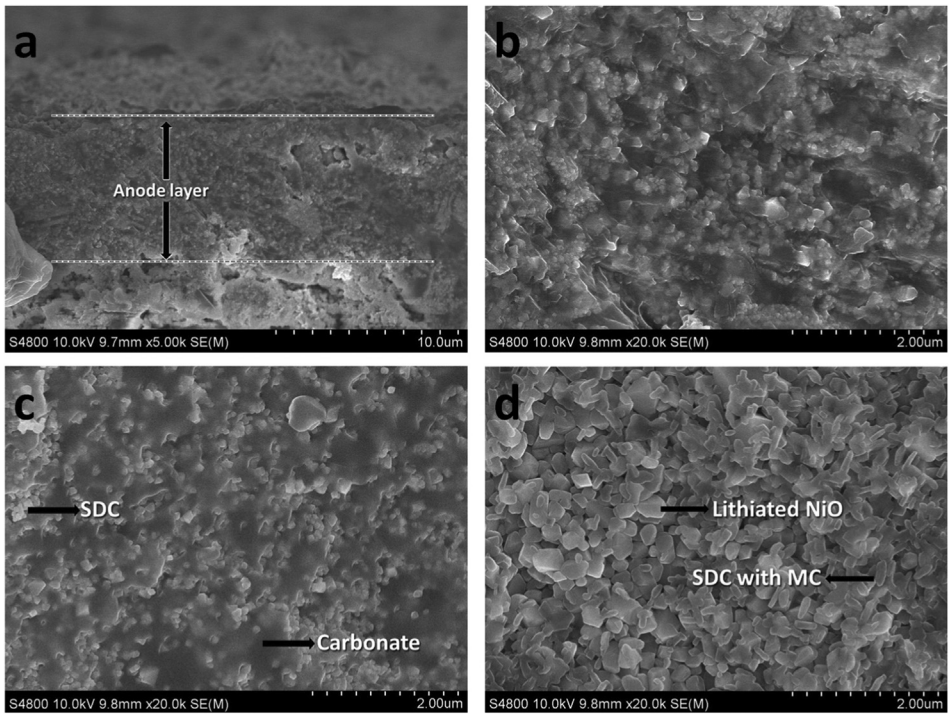

Fig. 4. SEM images of the fuel cell materials. (a) anode-electrolyte cross section part of the cell pellet, (b) anode layer, (c) composite electrolyte layer, (d) cathode layer.

3.2.2. Anode off-gas analysis

The anode off-gas of the fuel cell in the open circuit condition was analyzed by GC and the mole ratios of CO_2 and CO in the gas product as a function of the temperature are shown in Fig. 5. The mole ratio of CO (R_{co}) goes higher with the increase of the temperature. Blow 650 °C, R_{co} is lower than 0.08, but when the temperature is above 700 °C, R_{co} is higher than 0.18. This is because higher temperature is beneficial to enhance the Boudouard reaction. Thus, CO_2 from the carbonate dissociation reaction is consumed, and CO is formed in the anode fuel slurry.

3.2.3. Cell resistance analysis

A.C. impedance spectra of the fuel cell at open circuit condition in a temperature range of 600–750 °C are plotted in Fig. 6. The overall cell resistance is consisted of two major parts, the ohmic resistance (R_o) and the total polarization resistance (R_p). The R_p value at low frequency is reduced by increasing the working temperature, as shown in Fig. 6(a), due to the improvement of anode and cathode activities, and the enhancement of the mass transfer of the carbon fuel and the cathode gas. Fig. 6(b) presents that the change of the R_o is not obvious when the temperature increases from 600 to 700 °C. However, when the temperature reaches 750 °C, the R_o is about 0.17 Ω, 0.03 Ω less than that at below 700 °C. Above 700 °C, with the increase of the temperature, more CO is produced through the Boudouard reaction in the anode, which facilitates the reduction of NiO to Ni, leading to an enhanced electronic conductivity of the anode and an improved electrochemical performance.

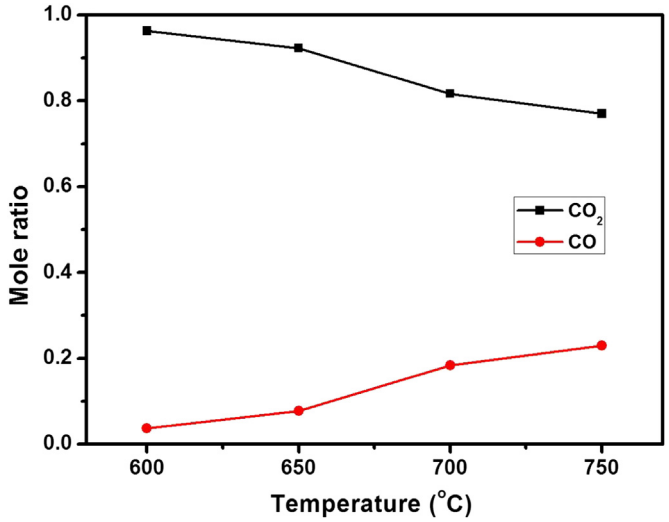

Fig. 5. Anode off-gas analysis of the fuel cell in the open circuit condition.

3.2.4. Power output

The *I–V* curves of the DCFC in the temperature range of 600–750 °C are presented in Fig. 7(a). The OCV of the cell increases with the increase of the operating temperature, from 0.90 V at 600 °C to 1.05 V at 750 °C. The *I–V* curves are nearly linear at low current density, but when the current density approaches 360 mA cm^{-2} at 700 °C and 480 mA cm^{-2} at 750 °C, the concentration polarization of the carbon fuel appears, which limits the electrochemical performance of the fuel cell. The power output increases with the increase of the operating temperature, as shown in Fig. 7(b). At 700 °C, the peak power density reaches 113 mW cm^{-2} at a current density of 237 mA cm^{-2}, which is higher than the result obtained by using activated carbon from coconut as the fuel [18]. The maximal power density of 185 mW cm^{-2} is obtained at a current density of 340 mA cm^{-2} at 750 °C, suggesting that the biomass is a promising fuel for DCFCs. Li et al. [27,28] found that stirring in the anode enhances the three-phase boundary area and improves the fuel cell performance.

3.3. General discussion

A scheme of the DCFC is presented in Fig. 8. Carbonate exists both in the anode fuel slurry and the electrolyte layer. In the

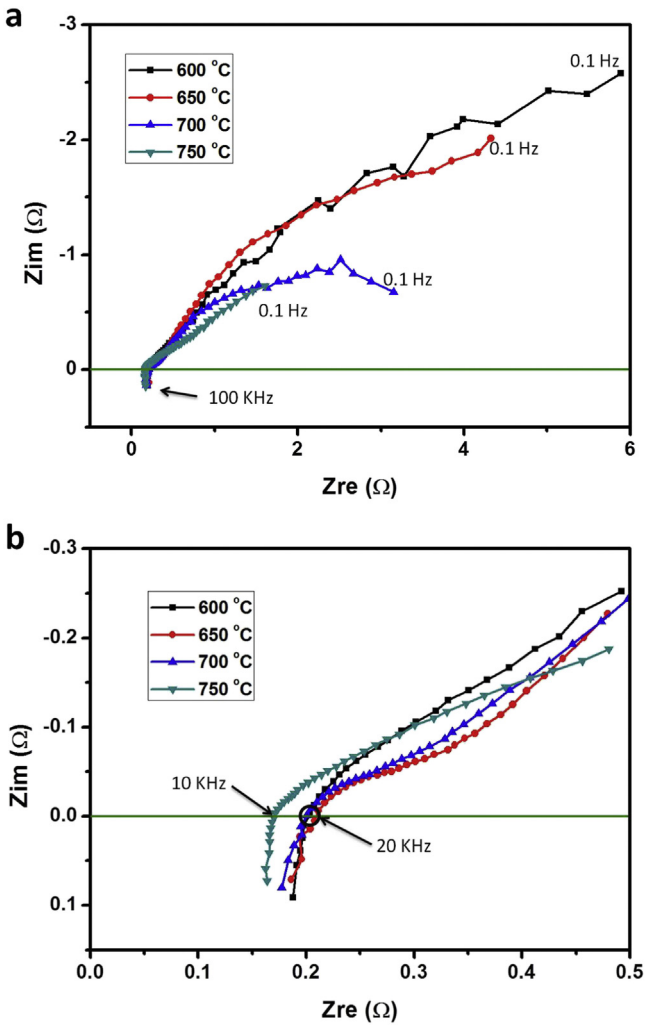

Fig. 6. (a) A.C. impedance spectra of the fuel cell at different temperature. (b) Zoom of the curves at low resistances and high frequency.

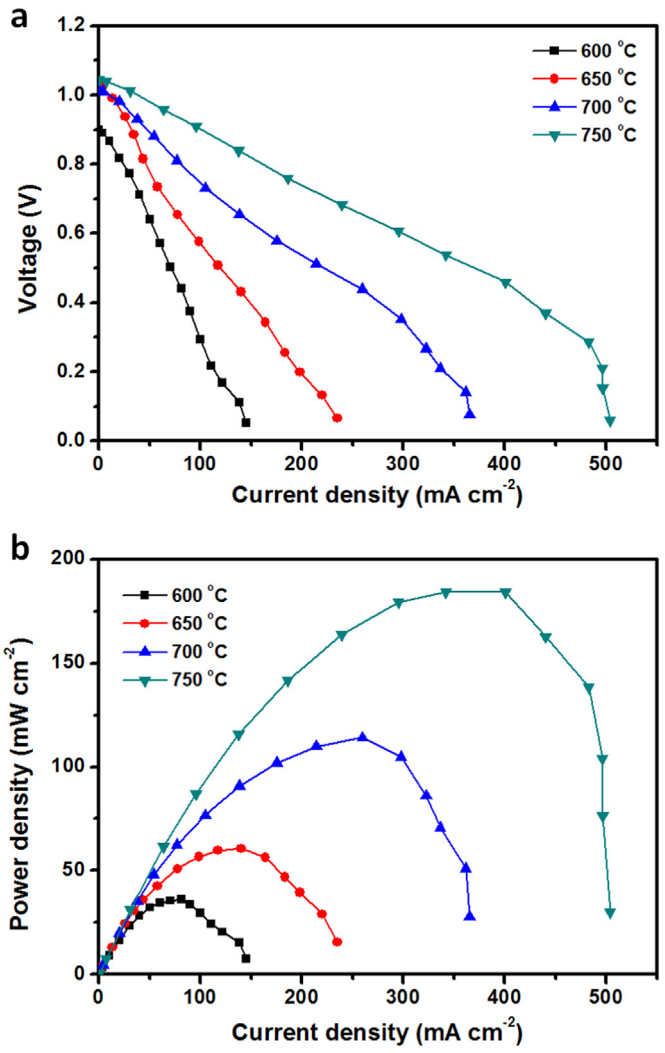

Fig. 7. Electrochemical performance of the biochar in DCFC at different temperature. (a) *I–V* curves, (b) *I–P* curves.

operation condition, the molten carbonate contacts well with the solid carbon fuel and enhances the diffusivity of the carbon to reach the reaction site. Meanwhile, the molten carbonate provides a high ionic conductivity at a relatively low temperature.

In our previous work [22], the CO formation in the chemical and electrochemical process was examined, however, we found that the CO formation was suppressed with the increase of the current density. In this work, CO is also measured in the anode off-gas and shows a trend of increase with the increase of temperature. In Fig. 8, we propose that Boudouard reaction plays an important role in the anode reaction cycle. However, in this work we cannot give direct supporting fact. In the early literature on DCFC, Cooper et al. [10] thought that carbon is oxidized directly by molten carbonate. Recently, Guo et al. [30] also found direct carbon electrochemical oxidation in the molten hydroxide fuel cell at low temperatures. Different reaction mechanism was proposed by Liu and coworkers [31]. They found that the anode reaction of a direct carbon SOFC is predominanted by the electrochemical oxidation of CO. Lee et al. [32] also assumed a similar CO oxidation mechanism in the direct carbon MCFC. Gür [13] suggested to use a name carbon fuel cell (CFC) instead of DCFC to describe the fuel cells combusting carbon, because he thought that the "direct" electrochemical oxidation of the solid carbon is difficult. CO acts as an important fuel participating in the electrochemical processes in the DCFC anode reaction especially at high temperatures.

4. Conclusion

In this work, the electrochemical performance of a biochar derived from corn cob has been examined as the fuel of a DCFC with

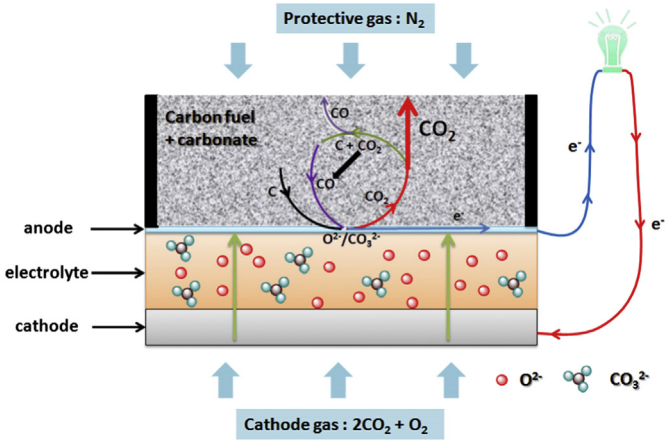

Fig. 8. A schematic diagram of DCFC with an SDC-carbonate electrolyte.

an SDC/carbonate electrolyte. The biochar from the pyrolysis of corn cob has a porous structure, low degree of graphitization and high chemical oxidation activity. With the printed anode layer (a mixture of NiO and SDC), the cathode corrosion by the molten carbonate is suppressed and the fuel cell stability is improved. The cell resistance and power output are highly dependent on the operating temperature. A peak power density of 185 mW cm^{-2} at a working temperature of 750 °C is obtained, which is much higher than the results obtained with the other types of carbon fuel in similar conditions. The anode off-gas is analyzed with a gas chromatograph, and the mole ratio of CO goes higher with the increase of the temperature. Boudouard reaction is supposed to participate in the anode reaction cycle.

Acknowledgments

The financial support of NSF of China under contract number 21120102039, the support of Tianjin Municipal Science and Technology Commission under contract number 13JCZDJC26600, and the support of the Ministry of Education of China under contract number 20130032120023 are gratefully acknowledged. The work has been also supported by the Program of Introducing Talents to the University Disciplines under file number B06006, and the Program for Changjiang Scholars and Innovative Research Teams in Universities under file number IRT 0641.

References

[1] A. Corma, S. Iborra, A. Velty, Chem. Rev. 107 (2007) 2411–2502.
[2] A.J. Ragauskas, C.K. Williams, B.H. Davison, G. Britovsek, J. Cairney, C.A. Eckert, W.J. Frederick, J.P. Hallett, D.J. Leak, C.L. Liotta, J.R. Mielenz, R. Murphy, R. Templer, T. Tschaplinski, Science 311 (2006) 484–489.
[3] P.J. Crutzen, M.O. Andreae, Science 250 (1990) 1669–1678.
[4] N. Savage, Nature 474 (2011) S9–S11.
[5] S. Mayfield, Nature 476 (2011) 402–403.
[6] G.W. Huber, S. Iborra, A. Corma, Chem. Rev. 106 (2006) 4044–4098.
[7] A.V. Bridgwater, G.V.C. Peacocke, Renew. Sust. Energ. Rev. 4 (2000) 1–73.
[8] D. Mohan, C.U. Pittman, P.H. Steele, Energy Fuels 20 (2006) 848–889.
[9] S. Czernik, A.V. Bridgwater, Energy Fuels 18 (2004) 590–598.
[10] N.J. Cherepy, R. Krueger, K.J. Fiet, A.F. Jankowski, J.F. Cooper, J. Electrochem. Soc. 152 (2005) A80–A87.
[11] D.X. Cao, Y. Sun, G.L. Wang, J. Power Sources 167 (2007) 250–257.
[12] Q.H. Liu, Y. Tian, C. Xia, L.T. Thompson, B. Liang, Y.D. Li, J. Power Sources 185 (2008) 1022–1029.
[13] T.M. Gur, Chem. Rev. 113 (2013) 6179–6206.
[14] C. Li, Y. Shi, N. Cai, J. Power Sources 196 (2011) 4588–4593.
[15] B. Zhu, X.G. Liu, P. Zhou, X.T. Yang, Z.G. Zhu, W. Zhu, Electrochem. Commun. 3 (2001) 566–571.
[16] C. Xia, L. Li, Y. Tian, Q.H. Liu, Y.C. Zhao, L.J. Jia, Y.D. Li, J. Power Sources 188 (2009) 156–162.
[17] C. Xia, Y. Li, Y. Tian, Q.H. Liu, Z.M. Wang, L.J. Jia, Y.C. Zhao, Y.D. Li, J. Power Sources 195 (2010) 3149–3154.
[18] L.J. Jia, Y. Tian, Q.H. Liu, C. Xia, J.S. Yu, Z.M. Wang, Y.C. Zhao, Y.D. Li, J. Power Sources 195 (2010) 5581–5586.
[19] H.J. Li, Q.H. Liu, Y.D. Li, Electrochim. Acta 55 (2010) 1958–1965.
[20] C.R. Jiang, J.J. Ma, A.D. Bonaccorso, J.T.S. Irvine, Energy Environ. Sci. 5 (2012) 6973–6980.
[21] A. Elleuch, J.S. Yu, A. Boussetta, K. Halouani, Y.D. Li, Int. J. Hydrogen Energy 38 (2013) 8514–8523.
[22] J. Yu, B. Yu, Y. Li, Int. J. Hydrogen Energy 38 (2013) 16615–16622.
[23] A. Elleuch, A. Boussetta, J.S. Yu, K. Halouani, Y.D. Li, Int. J. Hydrogen Energy 38 (2013) 16590–16604.
[24] A. Elleuch, A. Boussetta, K. Halouani, Y.D. Li, Int. J. Hydrogen Energy 38 (2013) 16605–16614.
[25] A. Elleuch, M. Sahraoui, A. Boussetta, K. Halouani, Y.D. Li, J. Power Sources 248 (2014) 44–57.
[26] Y.C. Zhao, C. Xia, L.J. Jia, Z.M. Wang, H.J. Li, J.S. Yu, Y.D. Li, Int. J. Hydrogen Energy 38 (2013) 16498–16517.
[27] X. Li, Z.H. Zhu, J.L. Chen, R. De Marco, A. Dicks, J. Bradley, G.Q. Lu, J. Power Sources 186 (2009) 1–9.
[28] X. Li, Z.H. Zhu, R. De Marco, A. Dicks, J. Bradley, S.M. Liu, G.Q. Lu, Ind. Eng. Chem. Res. 47 (2008) 9670–9677.
[29] T.M. Gur, J. Electrochem. Soc. 157 (2010) B751–B759.
[30] L. Guo, J.M. Calo, E. DiCocco, E.J. Bain, Energy Fuels 27 (2013) 1712–1719.
[31] Y.M. Xie, Y.B. Tang, J. Liu, J. Solid State Electrochem. 17 (2013) 121–127.
[32] C.G. Lee, M.B. Song, Fuel Cells 12 (2012) 1042–1047.